Analytical theory of the shear Alfvén continuum in the presence of a magnetic island

C. R. Cook[1, a)] and C. C. Hegna[1]
Departments of Physics and Engineering Physics, University of Wisconsin-Madison, Madison, WI 53706, USA

(Dated: 2 April 2015)

The effect of a magnetic island chain on the shear Alfvén continuum is calculated analytically. Using a WKB approximation of the linearized ideal MHD equations, the island is shown to cause an upshift in the continuum accumulation point frequency. This minimum of the frequency spectrum is shifted from the rational surface to the island separatrix. The structure of the eigenmodes is also presented.

I. INTRODUCTION

Most theoretical descriptions of the Alfvénic spectrum rely on the existence of topologically toroidal flux surfaces. In this work, the effects of a magnetic island on the shear Alfvén continuum are calculated using a WKB approximation. The analytic theory predicts an upshift in the continuum accumulation point frequency with the minimum value of the spectrum occuring at the island separatrix.

The shear Alfvén spectrum will become increasingly important as the fusion community pushes ahead towards ITER, and eventually DEMO. In particular, the presence of continuum gaps must be understood, as they can point to locations in the plasma where discrete Alfvén eigenmodes (AEs) could exist. These modes cannot couple to the Alfvén waves of the continuous spectrum and thus do not experience continuum damping. In high temperature fusion-relevant plasmas, these modes could potentially be driven unstable through a coupling to energetic α-particles. The speed of α-particles in ITER is predicted to be approximately $v_A < v_\alpha < 2v_A$, where v_A is the Alfvén velocity in ITER.[1]

The most commonly studied AEs in toroidal geometry include the Toroidicity-induced Alfvén Eigenmode (TAE) and the Beta-induced Alfvén Eigenmode (BAE). These modes lie in gaps that arise from a coupling of poloidal mode numbers and due to finite shear Alfvén wave compressibility via geodesic curvature coupling, respectively.[2,3]

Alfvén instabilities are a general feature of plasma equilibria that can occur in tokamaks, stellarators, and RFPs. As motivation for this work, MST recently observed a mode exhibiting Alfvénic scaling in 300kA, non-reversed plasmas with NBI.[4] Theoretical predictions using the STELLGAP code give a TAE gap frequency much higher than the observed mode frequency from experiment.[5] Conversely, the BAE gap frequency computed is lower than the experimental frequency seen on MST. A known limitation of the STELLGAP model is the assumption of closed, nested flux surfaces. A sizable $m = 1$, $n = 5$ island exists in the core of MST for these operating conditions which is not taken into account in these simulations. More recently, a BAE mode has been studied on the EAST tokamak. This mode is only present once an island width threshold has been reached, and appears to increase in frequency as the island evolves to a larger size.[6] Similar phenomena were originally observed on FTU[7,8] and TEXTOR.[9] With these experimental findings as motivation, it is natural to investigate whether an island can modify the Alfvén spectrum.

The effects of an island on the shear Alfvén continuum have been studied in some detail by Biancalani et al.[10–12] In Biancalani's work, a shooting method code was used to compute the spectrum. Biancalani showed that an island induces an upshift in the spectrum's minimum continuum accumulation point frequency. In the absence of an island, the spectrum minimum lies at the rational surface. In an equilibrium with an island, the location of the minimum shifts to the separatrix and the minimum frequency increases. In the following manuscript, analytic theory is employed to investigate these findings.

In this work, the equations for the shear Alfvén continuum are solved using WKB theory. The frequency upshift of the continuum accumulation point is demonstrated analytically for the first time, and matches previous numerical results by Biancalani. The paper is laid out as follows: in the next section an island coordinate system is introduced. These coordinates are needed to solve the Alfvén spectrum when an island is present. Section III describes the linearized ideal MHD model equations for an equilibrium with an island. The WKB analysis is detailed in the fourth section. The frequency continuum and eigenmode solutions are covered in Section V, followed by a summary and future outlook.

II. ISLAND COORDINATE SYSTEM

In order to obtain the Alfvén continuum, a straight field-line representation of the equilibrium magnetic field that includes the island has been employed.[13,14] The portion of the field without an island is represented in straight field line coordinates as $\mathbf{B_0} = q\nabla\psi \times \nabla\theta + \nabla\zeta \times \nabla\psi$, where ψ is the poloidal flux and θ and ζ are the poloidal and toroidal coordinates respectively; q is the safety factor. A symmetry-breaking magnetic field of the form $\sqrt{g}\mathbf{B_1} \cdot \nabla\psi = n_0 A \sin(m_0\theta - n_0\zeta)$ causes an island

a)cook@physics.wisc.edu

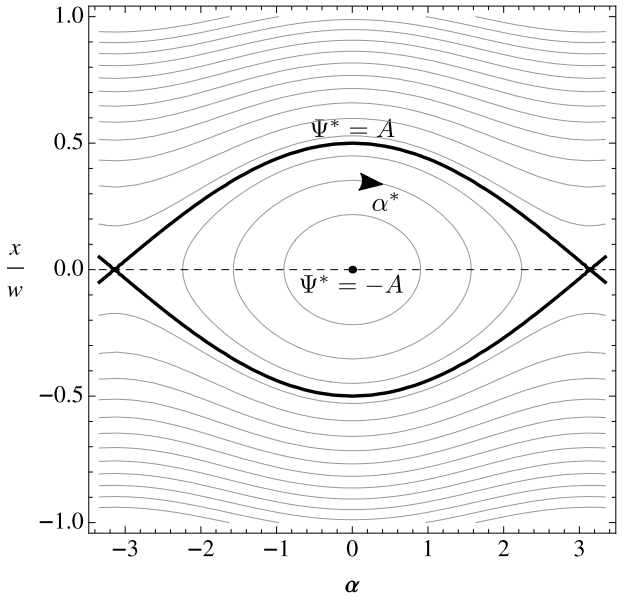

FIG. 1. Island coordinate system for $n_0 = 1$. Surfaces of constant Ψ^*/constant Φ^* appear as contours in the plot.

to form at $q(\psi_0) = q_0 = m_0/n_0$. Here, the Jacobian is $\sqrt{g} = (\nabla\psi \times \nabla\theta \cdot \nabla\zeta)^{-1}$. The constant-$\psi$ approximation of tearing mode analysis is utilized in this work, allowing us to treat A as a constant throughout the island region.[15]

A coordinate transformation to (Ψ^*, χ, α) space given by

$$\Psi^* = \int d\psi(q - q_0) - A\cos(n_0\alpha) \approx q_0' \frac{x^2}{2} - A\cos(n_0\alpha), \quad (1)$$

$$\chi = \theta, \quad (2)$$

$$\alpha = \zeta - q_0\theta, \quad (3)$$

is employed as a first step to derive a straight field representation for the total magnetic field. Here $x = \psi - \psi_0$ is the distance from the rational surface and $q_0' = dq/d\psi|_{\psi=\psi_0}$. The magnetic island width is given by $w = 4\sqrt{|A/q_0'|}$, and the island width will be considered small compared to equilibrium scales throughout this analysis, $\epsilon = q_0' w/2 \ll 1$. Ψ^* is a flux surface label, $\mathbf{B} \cdot \nabla\Psi^* = 0$ for the equilibrium in the presence of an island. See Fig. 1 for a visualization of the island coordinates. The island O-point is located at $\Psi^* = -A$ and the separatrix is at $\Psi^* = A$.

This transformation allows the total equilibrium field including the magnetic island $\mathbf{B} = \mathbf{B_0} + \mathbf{B_1}$ to be written as

$$\mathbf{B} = \nabla\alpha \times \nabla\psi + \nabla\Psi^* \times \nabla\chi. \quad (4)$$

Next, the coordinates $\Phi^* = \Phi^*(\Psi^*)$ (which also labels flux surfaces) and α^*, a helical angle in the reference frame of the island with $(0, 2\pi)$ periodicity on each helical flux surface, are defined such that

$$\nabla\alpha \times \nabla\psi = \nabla\alpha^* \times \nabla\Phi^*, \quad (5)$$

$$\frac{\partial x}{\partial\Phi^*} = \frac{\Omega}{q_0' x}, \quad (6)$$

$$\frac{\partial\alpha}{\partial\alpha^*} = \frac{q_0' x}{\Omega}. \quad (7)$$

The definitions of Φ^* and α^* inside and outside the island separatrix are presented in Appendix A. The island rotational transform Ω introduced here can be computed with the following:

$$\Omega(\Psi^*) = \frac{d\Psi^*}{d\Phi^*} = \frac{1}{\oint \frac{n_0 d\alpha}{2\pi}\left[1/\frac{\partial\Psi^*}{\partial x}\right]}. \quad (8)$$

Here, the distance x from the rational surface can be written in terms of Ψ^* and α as $x = \pm\sqrt{2/q_0'(\Psi^* + A\cos(n_0\alpha))}$.

Outside the island separatrix, $|\Psi^*| > A$, it is useful to define a flux surface label $k^2 = 2A/(|\Psi^*| + A)$. In this parameter, the separatrix is located at $k = 1$. The island rotational transform outside the island is given by

$$\Omega = \pm\frac{\pi\epsilon}{2kK(k^2)}, \quad (9)$$

where $\epsilon = q_0' w/2$ is the island half width (our small parameter) and $K(k^2)$ is the complete elliptic integral of the first kind. The plus and minus signs correspond to surfaces with $x > 0$ ($\psi > \psi_0$) and $x < 0$ ($\psi < \psi_0$), respectively.

Inside the island, $-A < \Psi^* < A$, we will label flux surfaces with $\kappa^2 = (\Psi^* + A)/2A$. The O-point is at $\kappa = 0$ and the separatrix is at $\kappa = 1$. Written with this surface label, the island rotational transform inside the magnetic island is the following:

$$\Omega(\Psi^*) = \frac{\pi\epsilon}{4K(\kappa^2)}. \quad (10)$$

Fig. 2 displays the helical rotational transform both inside and outside the island.

Using this island coordinate system, the total magnetic field can be written in a straight field form as

$$\mathbf{B} = \mathbf{B_0} + \mathbf{B_1} = \nabla\alpha^* \times \nabla\Phi^* + \Omega\nabla\Phi^* \times \nabla\chi. \quad (11)$$

This allows us to write the derivative along the magnetic field line in a much simpler form:

$$\mathbf{B} \cdot \nabla\lambda = \frac{1}{\sqrt{g}}\left[\frac{\partial\lambda}{\partial\chi} + \Omega\frac{\partial\lambda}{\partial\alpha^*}\right]. \quad (12)$$

This parallel gradient operator will be used in the next section when deriving the model equations.

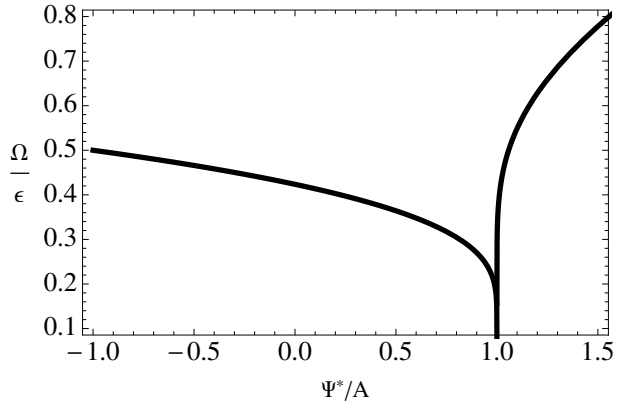

FIG. 2. Island rotational transform inside and outside the island. Note that $\Omega \to 0$ at the separatrix, $\Psi^* = A$.

III. IDEAL MHD IN THE PRESENCE OF AN ISLAND

In order to study the Alfvén spectrum in the vicinity of an island, a linearized ideal MHD model has been implemented. Throughout this manuscript, an equilibrium with a finite-sized magnetic island will be assumed. This is reflected in the equilibrium magnetic field representation $\mathbf{B} = \nabla\alpha^* \times \nabla\Phi^* + \Omega\nabla\Phi^* \times \nabla\chi$ derived in the last section. The equilibrium quantities satisfy force balance, Ampére's Law, and the divergence constraint:

$$\mathbf{J} \times \mathbf{B} = \nabla p, \tag{13}$$

$$\nabla \times \mathbf{B} = \mathbf{J}, \tag{14}$$

$$\nabla \cdot \mathbf{B} = 0. \tag{15}$$

The linearized ideal MHD equations are the momentum equation, the combined Faraday's law/Ohm's law, and the equation of state (natural units for plasmas, $\mu_0, \epsilon_0 = 1$, will be used throughout this paper). The linear system of equations for the MHD displacement vector $\boldsymbol{\xi}$, magnetic field perturbation $\boldsymbol{\delta}\mathbf{B}$, and pressure perturbation δp is given by

$$-\rho\omega^2\boldsymbol{\xi} = (\nabla \times \mathbf{B}) \times \boldsymbol{\delta}\mathbf{B} + (\nabla \times \boldsymbol{\delta}\mathbf{B}) \times \mathbf{B} - \nabla\delta p, \tag{16}$$

$$0 = \delta p + \boldsymbol{\xi} \cdot \nabla p + \gamma p \nabla \cdot \boldsymbol{\xi}, \tag{17}$$

$$\boldsymbol{\delta}\mathbf{B} = \nabla \times (\boldsymbol{\xi} \times \mathbf{B}). \tag{18}$$

Following Cheng and Chance's treatment, using the variables $\nabla \cdot \boldsymbol{\xi}$, $\xi_{\Phi^*} = \boldsymbol{\xi} \cdot \nabla\Phi^*$, $\delta P = \delta p + \boldsymbol{\delta}\mathbf{B} \cdot \mathbf{B}$, and the perpendicular surface component of the MHD displacement $\xi_s = \boldsymbol{\xi} \cdot (\mathbf{B} \times \nabla\Phi^*)/|\nabla\Phi^*|^2$, the ideal MHD eigenmode equations can be written in matrix form as[16]

$$\nabla\Phi^* \cdot \nabla \begin{bmatrix} \delta P \\ \xi_{\Phi^*} \end{bmatrix} = C \begin{bmatrix} \delta P \\ \xi_{\Phi^*} \end{bmatrix} + D \begin{bmatrix} \xi_s \\ \nabla \cdot \boldsymbol{\xi} \end{bmatrix}, \tag{19}$$

$$E \begin{bmatrix} \xi_s \\ \nabla \cdot \boldsymbol{\xi} \end{bmatrix} = F \begin{bmatrix} \delta P \\ \xi_{\Phi^*} \end{bmatrix}, \tag{20}$$

where C,D,E, and F are complicated operators containing only surface derivatives. The Alfvén and sound continua arise from solutions with a non-square-integrable singular radial structure. These solutions occur when the operator E does not have an inverse. Thus to find these continuum modes and their eigenfrequencies, ω^2, which compose the spectrum, the following system must be solved for every surface in the domain:

$$E \begin{bmatrix} \xi_s \\ \nabla \cdot \boldsymbol{\xi} \end{bmatrix} = 0. \tag{21}$$

For a cylindrical equilibrium with an island, the geodesic curvature given by $\kappa_s = 2\boldsymbol{\kappa} \cdot (\mathbf{B} \times \nabla\psi/B^2)$ is zero and the Alfvén and acoustic continua decouple. The general eigenmode equation for the shear Alfvén waves from Eq. (21) is then

$$\omega^2\rho\frac{|\nabla\Phi^*|^2}{B^2}\xi_s + \mathbf{B} \cdot \nabla\left(\frac{|\nabla\Phi^*|^2}{B^2}\mathbf{B} \cdot \nabla\xi_s\right) = 0. \tag{22}$$

In a general toroidal equilibrium with $\kappa_s \neq 0$, the two equations in Eq. (21) give a coupling of the Alfvén and sound waves. When the slow sound approximation $\gamma p/\omega^2\rho \ll 1$ is employed on these coupled equations, one arrives at the same Alfvén continuum equation as Eq. (22), but with a finite frequency upshift $\omega^2 \to \omega^2 - \omega^2_{BAE-CAP}$.[17,18] This frequency offset is known as the BAE-CAP (continuum accumulation point) frequency. In the absence of an island this minimum continuum frequency occurs at the rational surface where $\mathbf{B} \cdot \nabla \sim (m_0 - n_0 q) = 0$; this minimum frequency is zero for a cylinder. For the work that follows we will use ω^2 in Eq. (22), but everything can be generalized to a torus in the slow sound wave limit by replacing ω^2 with $\omega^2 - \omega^2_{BAE-CAP}$.

If we assume that the surface displacement can be described with a quantum number l in the island direction χ, $\xi_s(\chi, \alpha^*) = \xi_0(\alpha^*)\exp(il\chi)$, then the parallel gradient operator given by Eq. (12) can be written as

$$\begin{aligned}\mathbf{B} \cdot \nabla\xi_s &= \frac{1}{\sqrt{g}}\left(\Omega\frac{\partial}{\partial\alpha^*} + il\right)\xi_s \\ &= \frac{1}{\sqrt{g}}e^{\frac{-il}{\Omega}\alpha^*}\Omega\frac{\partial}{\partial\alpha^*}\left(\xi_s e^{\frac{il}{\Omega}\alpha^*}\right).\end{aligned} \tag{23}$$

Substituting this back into Eq. (22) results in

$$\frac{d}{d\alpha^*}\left(|\nabla\Phi^*|^2\frac{d}{d\alpha^*}Y\right) + \omega^2\rho\frac{\sqrt{g}^2}{\Omega^2}|\nabla\Phi^*|^2 Y = 0, \tag{24}$$

where we have set $Y = \xi_0(\alpha^*)\exp(il\alpha^*/\Omega)$. Thus a second-order ODE for the Alfvén eigenspectrum is obtained for each flux surface in the presence of a magnetic island.

IV. WKB ANALYSIS OF CONTINUUM EQUATION

The result derived in the last section, Eq. (24), can be rewritten with the identification $|\nabla\Phi^*|^2 =$

$(q_0' x/\Omega)^2 |\nabla\psi|^2$ and a normalized frequency given by $\hat{\omega}^2 = \omega^2/\omega_A^2$. Here the Alfvén frequency is $\omega_A = 1/\sqrt{\rho}\sqrt{g}$. Employing these definitions simplifies the eigenmode equation as follows:

$$\frac{d}{d\alpha^*}\left[x^2 \frac{d}{d\alpha^*} Y\right] + \frac{\hat{\omega}^2 x^2}{\Omega^2} Y = 0. \tag{25}$$

From Eq. (25), the frequency $\hat{\omega}^2$ can be shown to be positive:

$$\hat{\omega}^2 = \Omega^2 \frac{\oint d\alpha^* x^2 \left|\frac{dY}{d\alpha^*}\right|^2}{\oint d\alpha^* x^2 |Y|^2} \geq 0. \tag{26}$$

Thus the square of the Alfvén spectrum frequencies cannot be negative, meaning the spectrum is stable. In the following, we will show that the presence of the island causes a non-zero upshift to the minimum frequency.

Eq. (25) can be written in terms of a dimensionless distance from the rational surface, $\hat{x} = \sqrt{\kappa^2 - \sin^2 n_0\alpha/2}$ where $x = (w/2)\hat{x}$. This results in our final form of the continuum equation, cast in Schrödinger form:

$$\frac{\Omega^2}{\hat{\omega}^2}\hat{x}^2 \frac{d}{d\alpha^*}\left[\hat{x}^2 \frac{d}{d\alpha^*} Y\right] + \hat{x}^4 Y = 0. \tag{27}$$

The representation of $\hat{x}$ in α^*-space is included in Appendix A. In this paper we will consider $l = 0$ in $\xi_s = Y(\alpha^*)\exp[il(\chi - \alpha^*/\Omega)]$, so our solutions are equal to the surface displacements, $Y = \xi_s$. Our boundary conditions are periodic in α^*:

$$Y(\alpha^*) = Y(\alpha^* + 2\pi), \tag{28}$$

$$\left.\frac{dY}{d\alpha^*}\right|_{\alpha^*} = \left.\frac{dY}{d\alpha^*}\right|_{\alpha^*+2\pi}. \tag{29}$$

Eq. (27) lends itself to a WKB analysis. Comparing the equation to the canonical Schrödinger equation

$$\delta^2 \frac{d^2 Y}{dt^2} - Q(t) Y = 0, \tag{30}$$

gives the following identifications:

$$Q = -\hat{x}^4, \tag{31}$$

$$\delta = \frac{\Omega}{\hat{\omega}}, \tag{32}$$

$$\frac{d\alpha^*}{dt} = \hat{x}^2. \tag{33}$$

The formal WKB expansion for the solution is $Y \sim \exp[(1/\delta)\sum \delta^n S_n(t)]$, where the summation is from $n = 0$ to ∞ and the small parameter $\delta \sim \Omega \sim \epsilon$. Inserting this expansion into the general Schrödinger equation and solving to second order gives the following solutions for S_0, S_1, and S_2 in terms of the potential Q:

$$S_0 = \pm \int \sqrt{Q} dt, \tag{34}$$

$$S_1 = -\frac{1}{4}\log Q, \tag{35}$$

$$S_2 = \pm \int \left[\frac{Q''}{8Q^{3/2}} - \frac{5(Q')^2}{32Q^{5/2}}\right] dt. \tag{36}$$

Inserting $Q = -\hat{x}^4$ into the lowest two orders and working out the details gives

$$S_0 = \pm i\alpha^*, \tag{37}$$

$$S_1 = -\frac{1}{4}\log(-\hat{x}^4), \tag{38}$$

The specific form of S_2 is presented in Appendix A for surfaces both inside and outside the separatrix.

Substituting S_0, S_1, and S_2 into $Y \sim \exp[S_0/\delta + S_1 + \delta S_2]$ results in the following WKB solution:

$$Y \sim \frac{1}{\hat{x}} e^{\pm i\left(\frac{\hat{\omega}}{\Omega}\alpha^* + \frac{\Omega}{\hat{\omega}}\hat{S}_2(\alpha^*)\right)}. \tag{39}$$

Here $S_2(\alpha^*) = \pm i\hat{S}_2(\alpha^*)$. The plus and minus signs correspond to two linearly independent solutions for the second-order ODE. These two solutions can be combined to form odd and even solutions given by the following:

$$Y_O \sim \frac{1}{\hat{x}} \sin\left(\frac{\hat{\omega}}{\Omega}\alpha^* + \frac{\Omega}{\hat{\omega}}\hat{S}_2(\alpha^*)\right), \tag{40}$$

$$Y_E \sim \frac{1}{\hat{x}} \cos\left(\frac{\hat{\omega}}{\Omega}\alpha^* + \frac{\Omega}{\hat{\omega}}\hat{S}_2(\alpha^*)\right). \tag{41}$$

With this result, we will derive the structure of the eigenmodes and the corresponding shear Alfvén eigenspectrum in the next section.

V. ALFVÉN CONTINUUM AND EIGENMODE STRUCTURE

The solutions from Eqs. (40) and (41) can be made consistent with the periodic boundary conditions given in Eqs. (28) and (29). The resulting continuum frequencies are given by

$$\hat{\omega}^2 = \left[\frac{j\Omega}{2} + \sqrt{\left(\frac{j\Omega}{2}\right)^2 + \frac{q_0'}{2}\left(\Psi^* - \frac{1}{2}\Omega\Phi^*\right)}\right]^2, \tag{42}$$

where j is a positive integer. We will see that outside the separatrix, $j = j_{out}$ where $j_{out} = 1, 2, 3, ...$ is the quantum number. Inside the separatrix, $j = n_0(j_{in} + 1)$ where $j_{in} = 1, 2, 3, ...$ is the quantum number for the interior region of the island. Eq. (42) represents the shear Alfvén eigenspectrum, valid for surfaces inside and outside the separatrix. In order to investigate the nature of the eigenmodes, we will consider surfaces both inside and outside the separatrix.

For flux surfaces outside the island, the envelope function $1/\hat{x}$ of the solution remains well-behaved since $\hat{x}$ does not pass through zero. Due to this, modes of both parities are allowed for all quantum numbers outside the separatrix, giving us the following eigenmodes outside the island:

$$Y_O^j = \frac{1}{\sqrt{\pi}\hat{x}(\alpha^*)} \sin\left[j_{out}\alpha^*\right], \tag{43}$$

$$Y_E^j = \frac{1}{\sqrt{\pi}\hat{x}(\alpha^*)} \cos\left[j_{out}\alpha^*\right]. \tag{44}$$

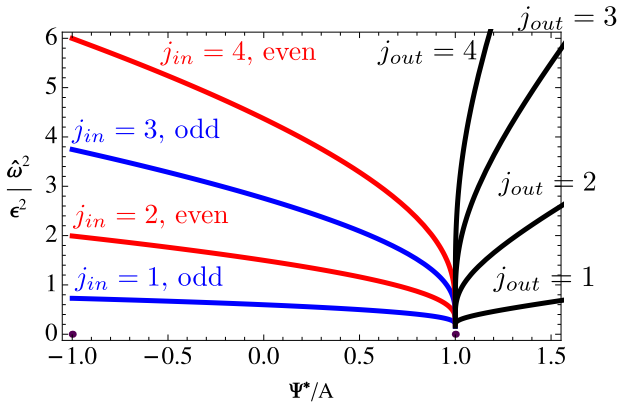

FIG. 3. Shear Alfvén continuum in the presence of a magnetic island. Inside the separatrix, the frequencies of the odd modes are blue curves while the even modes are red. Outside the separatrix, both parities exist at the same frequency.

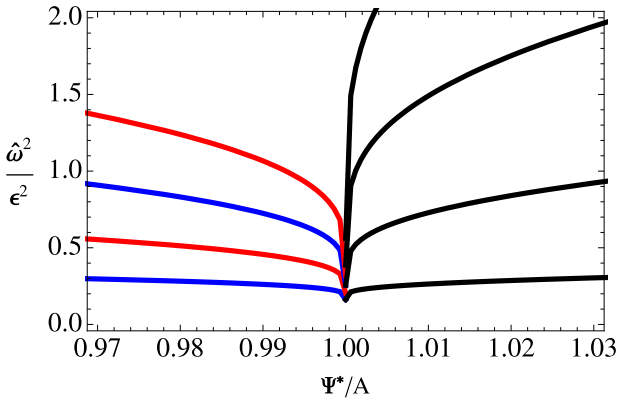

FIG. 4. Shear Alfvén continuum behavior near the separatrix ($\Psi^* = A$). Note that all branches of the continuum limit to a non-zero frequency at the separatrix, $\hat{\omega}^2_{sep}/\epsilon^2 = 1/8$.

Here the quantum number $j_{out} = 1, 2, 3, ...$ The coefficient comes from the normalization condition, $\oint d\alpha^* \hat{x}^2 |Y|^2 = 1$.

For surfaces within the island, the envelope of the solutions contains an apparent $1/\hat{x}$ singularity occuring when $\hat{x} = 0$ at $\alpha^* = \pi/2n_0$. This singularity can be removed by forcing the trig functions in Eqs. (40) and (41) to zero at $\alpha^* = \pi/2n_0$. Under this constraint we lose half of the solutions inside the island, and our eigenmodes are odd for j_{in} odd and even for j_{in} even:

$$Y^j_O = \frac{1}{\sqrt{\pi}\hat{x}(\alpha^*)} \sin\left[n_0(j_{in}+1)\alpha^*\right], \; j_{in} = 1, 3, 5, .. \quad (45)$$

$$Y^j_E = \frac{1}{\sqrt{\pi}\hat{x}(\alpha^*)} \cos\left[n_0(j_{in}+1)\alpha^*\right], \; j_{in} = 2, 4, 6, .. \quad (46)$$

Now that we have the equation for the shear Alfvén continuum and the corresponding continuum modes, we can look at the structure of the spectrum. The Alfvén eigenspectrum given by Eq. (42) is plotted in Fig. 3. Note that Eq. (27) can be solved analytically at the O-point ($\Psi^* = -A$), resulting in $(\hat{\omega}/\epsilon)^2 = [n_0^2(j_{in}+1)^2 - 1]/4$. This agrees well with our second-order WKB approximated solution at the O-point plotted in Fig. 3.

Two zero frequency modes, $\hat{\omega}^2 = 0$, have been included in the figure as purple points; one is located at the O-point and the other at the X-point of the separatrix. The solution $\hat{\omega}^2 = 0$ with Y a constant is a known, trivial solution to the Alfvén eigenmode equation for any magnetic geometry and is generally not included. It is usually neglected because the quantum numbers are zero which makes the eigenmode a constant. It is included and important at the singular O- and X-points here because in the original θ and ζ coordinates from the toroidal magnetic field, the quantum numbers are non-zero. Indeed, the zero frequency behavior at the O-point and X-point corresponds to $m = m_0$, $n = n_0$. This means that the O-point and X-point retain the marginal stability ($\hat{\omega}^2 = 0$) inherent in the original resonant, rational surface ψ_0. As such, the O-point and X-point will still be only marginally stable to $m = m_0$ and $n = n_0$ perturbations.

The behavior of the spectrum near the separatrix ($\Psi^* = A$) is of considerable interest. Since the rotational transform Ω goes to zero at the separatrix, $\delta = \Omega/\hat{\omega} \to 0$, the WKB expansion is formally valid for all finite j at the separatrix. Fig. 4 provides a close-up of the spectrum for surfaces near the separatrix. It can be seen that all of the frequencies converge to an island-modified, non-zero continuum accumulation point frequency at the separatrix. The value of this minimum frequency is

$$\left(\frac{\hat{\omega}_{sep}}{\epsilon}\right)^2 = \lim_{\Psi^* \to A} \left(\frac{\hat{\omega}}{\epsilon}\right)^2 = \frac{1}{8}. \quad (47)$$

This minimum frequency at the separatrix can be written out explicitly as $\omega^2_{sep} = (q_0' w)^2 \omega_A^2/32$. After transforming to the proper coordinates, this is the same frequency upshift that was previously found numerically by Biancalani.[12]

The lowest two eigenmodes for each parity outside the separatrix given by Eqs. (43) and (44) are plotted in Fig. 5 for $\Psi^* = 2A$ ($k^2 = 2/3$). The lowest two eigenmodes inside the separatrix given by Eqs. (45) and (46) are plotted in Fig. 6 for $\Psi^* = A/2$ ($\kappa^2 = 3/4$).

VI. SUMMARY

The shear Alfvén continuum for an equilibrium with an island has been obtained using a WKB analysis. A finite upshift in the continuum accumulation point frequency has been demonstrated analytically for the first time for modes with the same helicity as the magnetic island ($l = 0$). This result confirms past numerical simulations by Biancalani et al that show an increase in this minimum frequency of the spectrum as well as a movement of the location of this frequency from the rational surface to the island separatrix.[12] Specifically, the

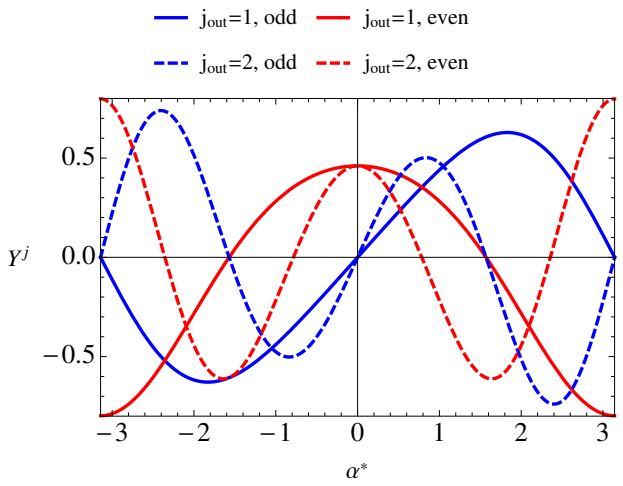

FIG. 5. $j_{out} = 1$ (solid) and $j_{out} = 2$ (dashed) mode structure for $\Psi^* = 2A$ surface outside the island. Outside the separatrix, even and odd parities are both present and degenerate in frequency.

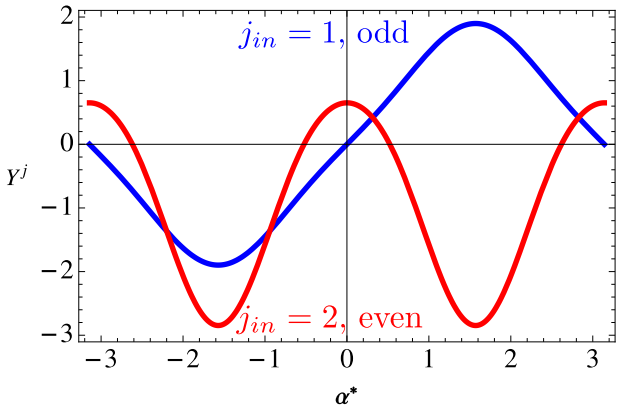

FIG. 6. $j_{in} = 1$ odd (blue) and $j_{in} = 2$ even (red) mode structure for $\Psi^* = A/2$ surface inside the island. Inside the separatrix, odd j_{in} correspond to odd modes and even j_{in} correspond to even modes.

WKB theory presented here predicts an upshift of the frequency to $\omega^2_{sep} = \omega^2_{BAE-CAP} + (q_0' w)^2 \omega_A^2/32$ for a toroidal equilibrium with finite κ_s (where we have let $\omega^2 \to \omega^2 - \omega^2_{BAE-CAP}$ as described in Section III). This frequency upshift also holds for a cylindrical equilibrium where $\omega_{BAE-CAP} = 0$.

The properties of the spectrum and modes for $l \neq 0$ will be studied in the future. This study will be compared to the results of Biancalani for $l \neq 0$.[10,11] In particular, secondary resonances are expected at rational Ω surfaces where $l_0 - j_0\Omega = 0$. Future work will also involve studying the Alfvén spectrum numerically using the SIESTA code.[19] SIESTA is a 3D MHD equilibrium code capable of resolving equilibria with islands. Once an equilibrium is computed, the continuum is obtained using the Hessian matrix of the potential energy, H, and the inertia matrix, T, from the SIESTA simulation. The generalized eigenvalue problem $H\boldsymbol{\xi} = -\omega^2 T\boldsymbol{\xi}$ can then be solved, resulting in the Alfvén continuum. These computational studies can give further insight into the structure of the stable spectrum; they also could identify the possible existence of discrete Alfvén eigenmodes in the gaps of the spectrum. Preliminary comparisons with observations on MST show that the AE frequencies from the experiments are consistent with modes that lie in the gap induced by the magnetic island. A detailed comparison with MST data is outside the scope of this paper and will be pursued in future work.

ACKNOWLEDGMENTS

One of the authors (C. R. Cook) would like to acknowledge useful correspondence and help from A. Biancalani and D. A. Spong. This work is supported by the U.S. Department of Energy under grants DE-FG02-99ER54546 and DE-SC0006103.

Appendix A: Island coordinates

The island coordinates outside the separatrix are given by

$$\Phi^* = \pm\frac{w}{\pi k}E(k^2), \tag{A1}$$

$$\alpha^* = \frac{\pi}{n_0 K(k^2)}F\left(\frac{n_0\alpha}{2}, k^2\right), \tag{A2}$$

where $K(k^2)$ and $E(k^2)$ are the complete elliptic integrals of the first and second kind, respectively, and $F(n_0\alpha/2, k^2)$ is the incomplete elliptic integral of the first kind.

Inside the separatrix, we have

$$\Phi^* = \frac{2w}{\pi}\left[E(\kappa^2) + (\kappa^2 - 1)K(\kappa^2)\right], \tag{A3}$$

$$\alpha^* = \frac{\pi}{2n_0 K(\kappa^2)}F\left(\sin^{-1}\left[\frac{1}{\kappa}\sin\frac{n_0\alpha}{2}\right], \kappa^2\right). \tag{A4}$$

In terms of α^*, x outside and inside the separatrix, respectively, can be written as

$$\hat{x} = \sqrt{\frac{1}{k^2} - sn^2\left[\frac{n_0 K(k^2)}{\pi}\alpha^*, k^2\right]}, \tag{A5}$$

$$\hat{x} = \kappa cn\left[\frac{2n_0 K(\kappa^2)}{\pi}\alpha^*, \kappa^2\right]. \tag{A6}$$

Here, sn and cn are the Jacobi elliptic functions.

S_2 from the WKB expansion takes the following form,

outside and inside the separatrix:

$$S_2 = \pm \frac{i\epsilon}{4k\Omega}[(k^2-2)\frac{K(k^2)}{\pi}\alpha^* + 2E\left(am\left[\frac{K(k^2)}{\pi}\alpha^*, k^2\right], k^2\right)], \quad \text{(A7)}$$

$$S_2 = \pm \frac{i\epsilon}{8\Omega}[-\frac{4K(\kappa^2)}{\pi}\alpha^* + 4E\left(am\left[\frac{2K(\kappa^2)}{\pi}\alpha^*, \kappa^2\right], \kappa^2\right)]. \quad \text{(A8)}$$

In these expressions, am is the Jacobi amplitude and $E(\cdot, k^2)$ is the incomplete elliptic integral of the second kind.

REFERENCES

[1]N. N. Gorelenkov, E. Belova, H. L. Berk, C. Z. Cheng, E. Fredrickson, W. W. Heidbrink, S. Kaye, and G. J. Kramer, Phys. Plasmas, **11**, 2586 (2004).

[2]F. Zonca and L. Chen, Phys. Plasmas, **21**, 072120 (2014).

[3]F. Zonca and L. Chen, Phys. Plasmas, **21**, 072121 (2014).

[4]J. Koliner, C. Forest, J. Sarff, J. Anderson, D. Liu, M. Nornberg, J. Waksman, L. Lin, D. Brower, W. Ding, and D. Spong, Phys. Rev. Lett., **109**, 115003 (2012).

[5]D. A. Spong, E. DAzevedo, and Y. Todo, Phys. Plasmas, **17**, 022106 (2010).

[6]M. Xu, W. Chen, L. Q. Hu, R. J. Zhou, G. Q. Zhong, T. H. Shi, L. Q. Xu, Y. Zhang, Y. W. Sun, S. Y. Lin, and B. Shen, Plasma Phys. Control. Fusion, **55**, 065002 (2013).

[7]P. Buratti, P. Smeulders, F. Zonca, S. Annibaldi, M. D. Benedetti, H. Kroegler, G. Regnoli, O. Tudisco, and the FTU-team, Nucl. Fusion, **45**, 1446 (2005).

[8]S. V. Annibaldi, F. Zonca, and P. Buratti, Plasma Phys. Control. Fusion, **49**, 475 (2007).

[9]O. Zimmermann, H. R. Koslowski, A. Krämer-Flecken, Y. Liang, R. Wolf, and the TEC-team, Proceedings of the 32nd EPS Conference on Plasma Physics, Tarragona, Spain, **29C**, P4.059 (2005).

[10]A. Biancalani, L. Chen, F. Pegoraro, and F. Zonca, Phys. Plasmas, **17**, 122106 (2010).

[11]A. Biancalani, L. Chen, F. Pegoraro, and F. Zonca, Phys. Rev. Lett., **105**, 1 (2010).

[12]A. Biancalani, L. Chen, F. Pegoraro, and F. Zonca, Plasma Phys. Control. Fusion, **53**, 025009 (2011).

[13]C. C. Hegna and J. D. Callen, Phys. Fluids B Plasma Phys., **4**, 3031 (1992).

[14]C. C. Hegna, Plasma Phys. Control. Fusion, **53**, 024003 (2011).

[15]P. H. Rutherford, Phys. Fluids, **16**, 1903 (1973).

[16]C. Z. Cheng and M. S. Chance, Phys. Fluids, **29**, 3695 (1986).

[17]M. S. Chu, J. M. Greene, L. L. Lao, A. D. Turnbull, and M. S. Chance, Phys. Fluids B Plasma Phys., **4**, 3713 (1992).

[18]A. D. Turnbull, E. J. Strait, W. W. Heidbrink, M. S. Chu, H. H. Duong, J. M. Greene, L. L. Lao, T. S. Taylor, and S. J. Thompson, Phys. Fluids B Plasma Phys., **5**, 2546 (1993).

[19]S. P. Hirshman, R. Sanchez, and C. R. Cook, Phys. Plasmas, **18**, 062504 (2011).